Environmental Science & Technology

pubs.acs.org/est

Article

Tying up Loose Ends of Microplastic Pollution in the Arctic: Distribution from the Sea Surface through the Water Column to Deep-Sea Sediments at the HAUSGARTEN Observatory

Mine B. Tekman,* Claudia Wekerle, Claudia Lorenz, Sebastian Primpke, Christiane Hasemann, Gunnar Gerdts, and Melanie Bergmann

Cite This: *Environ. Sci. Technol.* 2020, 54, 4079−4090

Read Online

ACCESS | Metrics & More | Article Recommendations | Supporting Information

ABSTRACT: Recent studies have shown that despite its remoteness, the Arctic region harbors some of the highest microplastic (MP) concentrations worldwide. Here, we present the results of a sampling campaign to assess the vertical distribution of MP particles (>11 μm) at five stations of the HAUSGARTEN observatory. Water column samples were taken with large volume pumps by filtering 218−561 L of seawater at two to four depth strata (near-surface, ∼300 m, ∼1000 m, and above seafloor), and sediment samples were taken with a multiple corer. MP concentrations in the water column ranged between 0 and 1287 N m^{-3} and in the sediment from 239 to 13 331 N kg^{-1}. Fourier transform infrared spectroscopy (FTIR) imaging with automated data analysis showed that polyamide (39%) and ethylene-propylene-diene rubber (23%) were the most abundant polymers within the water samples and polyethylene-chlorinated (31%) in sediments. MPs ≤ 25 μm accounted for more than half of the synthetic particles in every sample. The largest MP particle recorded was in the 200 μm size class. The concentrations of fibers were not reported, as fiber detection by FTIR imaging was not available at the time of analyses. Two- and three-dimensional simulations of particle transport trajectories suggest different pathways for certain polymer types. A positive correlation between MP size composition and particulate organic carbon indicates interactions with biological processes in the water column.

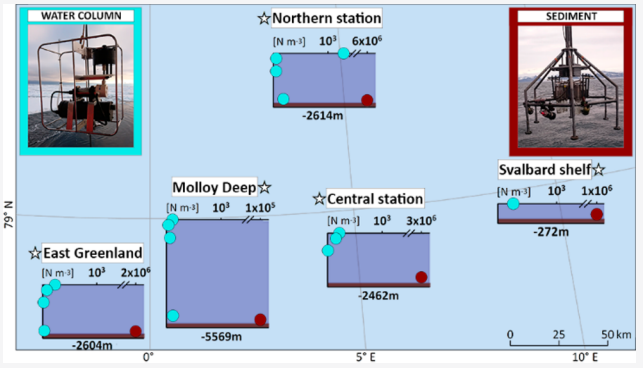

INTRODUCTION

Over the past decade, the pollution of our oceans with plastic has aroused great attention in both environmental research and public discourse.[1] The more research has been conducted, the more the extent of the problem has been unveiled.[2] Microplastic (MP) particles further complicate our comprehension of the problem because these small particles (<5 mm) have been observed throughout the world oceans,[3] including in sea ice,[4,5] on the deep seafloor,[2] and within biota.[6] Additionally, MP particles have not been found exclusively in the marine compartments of the global ecosystem but also within the atmosphere,[7,8] freshwater,[9] and terrestrial[10] environments. There is still uncertainty as to the scope and severity of any detrimental effects MP may have on organisms,[11] although some health implications have been identified.[12−14]

Rapid changes in the world's climate have drawn particular attention to the Arctic regions, where plastic pollution has, alongside environmental change, been recognized as a growing problem.[15,16] As a result of the recent research activities, our knowledge on plastic and MP pollution in the Arctic is improving.[17] However, within Arctic waters (and the world oceans in general), MP concentrations and transport pathways within the water column remain understudied. Concentrations reported from a limited number of water column studies have shown great variation in measured quantities,[18−21] although they indicate a ubiquitous presence in the water column globally. Moreover, MP has been suggested to incorporate into marine particles[22−30] and alter sinking velocities.[24,25,28] These findings are important in the context of the biological pump. The biological pump is the process by which photosynthetically produced organic matter is exported to the deep ocean via sinking particles, which are subjected during settling to advection, vertical mixing, and potential removal from the water column to organisms via consumption.[31] Given that this pump drives the food supply to the deep ocean,[32] it is crucial to understand how the presence of MP may affect the sinking

Received: November 18, 2019
Revised: March 4, 2020
Accepted: March 6, 2020
Published: March 6, 2020

Table 1. Microplastic Concentrations in Arctic Sediment and Water Samples Taken at Different Depths

station	realm	sampling depth (m)	sample volume (L) and dry weight (g)[a]	subsample volume for FTIR (%)	MP (N m^{-3})[b]	MP (N kg^{-1})
EGIV (78.8°N, 2.8°E)	water column	−1	218 L	100	227	
	water column	−303	490 L	55	78	
	water column	−993	556 L	77	16	
	water column	−2574	541 L	64	29	
	sediment	−2604	823 g	12	1.9×10^6	2437
N5 (79.9°N, 3.1°W)	water column	−3	223 L	5	1287	
	water column	−289	499 L	41	54	
	water column	−999	554 L	48	53	
	water column	−2549	546 L	27	186	
	sediment	−2614	513 g	4	6.3×10^6	13 331
HGIV (79.1°N, 4.2°W)	water column	−1	223 L	49	218	
	water column	−302	501 L	90	152	
	water column	−974	559 L	80	9	
	water column	−2449	546 L	26	0	
	sediment	−2462	582 g	5	3.2×10^6	5099
HGIX (79.1°N, 2.8°W)	water column	−2	228 L	35	113	
	water column	−308	496 L	6	38	
	water column	−1022	561 L	17	65	
	water column	−5350	542 L	11	119	
	sediment	−5569	509 g	52	0.1×10^6	239
SVI (79.0°N, 11.1°W)	water column	−1	424 L	100	262	
	water column	−250	544 L	64	0	
	sediment	−272	630 g	11	1.3×10^6	2542

[a]Sample volume (L) and dry weight (g) column represents total in situ filtered volume of the water samples and total weight of the sediment samples. [b]Sediment microplastic concentrations in N m^{-3} were calculated by multiplying the concentrations in N kg^{-1} with (dry) sediment density. The dry weight (wet weight × porosity) was divided by the volume of the subsample to obtain the sediment density (kg m^{-3}) at each station. Weight, volume, and porosity values were measured from additional sediment cores taken to analyze environmental parameters.

behavior and the efficiency of organic matter export pathways from the surface waters to the deep seafloor.

Aside from settling behavior and abundance, another important MP parameter is the size of the particles. MP particles of 10 μm may be transferred to upper trophic levels within the planktonic food web.[33] The majority of studies identifying and quantifying MP conducted to date via visual selection and subsequent verification by Fourier transform infrared spectroscopy (FTIR) allows the detection of particles >100 μm. FTIR imaging with a lower detection limit of 11 μm[34] has shown that particles ≤25 μm represent the highest proportion of MP particles in environmental samples, suggesting that there is no lower limit on MP size following fragmentation.[2,8,35,36] Therefore, it is plausible to assume that many hitherto reported environmental MP concentrations have underestimated abundances and potentially, size-related interactions of small MP particles (<100 μm) with organisms have gone unnoticed.

The Fram Strait is the only deep-water connection between the Arctic Ocean and the North Atlantic, characterized by contrasting water masses.[37] Warm Atlantic water entering the Fram Strait as West Spitzbergen Current (WSC) facilitates melting of sea ice and subsequent release of particles and organisms entrained, contributing to the downward flux of particles.[37] A fraction of the WSC recirculates at ∼79 °N and subducts underneath cold polar waters that exit the Arctic Ocean. The East Greenland Current (EGC) carries both of these water masses southward. This complex structure of currents from different origins affects the particle distribution locally within the water column.[37]

Here, we analyzed samples taken from near-surface waters, the deep water column and deep-sea sediments for MP (excluding fibers) at five stations of the HAUSGARTEN observatory. The distribution of MP particles was studied in the context of simulated particle trajectories and environmental parameters to investigate possible sources, transportation pathways, and accumulation mechanisms of MP in the Fram Strait. To this end, we assessed (i) the spatial distribution of MP particles among stations and depths, (ii) differences between the water column and sediments, (iii) possible interactions with the biological pump, (iv) effect of sea ice on the MP distribution, and (v) potential source areas of MP particles.

MATERIALS AND METHODS

Sampling Procedure. Water and sediment sampling were conducted in the summer of 2016 during *RV Polarstern* expedition PS99.2 to the HAUSGARTEN observatory. In 1999, the Alfred Wegener Institute Helmholtz Centre for Polar and Marine Research (AWI) initiated the long-term ecological research (LTER) observatory HAUSGARTEN in the Fram Strait.[38] Twenty-one stations along a bathymetric and latitudinal gradient have been sampled annually to assess the effects of climate change on faunal, bacterial, biogeochemical, geological, hydrographic, and sedimentation processes. Four

https://dx.doi.org/10.1021/acs.est.9b06981
Environ. Sci. Technol. 2020, 54, 4079−4090

deep stations and one shallow station from the HAUSGARTEN observatory were selected for the current study, covering the full range of oceanographic regimes found in the Fram Strait. These stations were (1) EGIV, located in the East Greenland Current (2604 m depth); (2) N5, the closest station to the marginal ice zone (2614 m depth); (3) the Molloy Deep (HGIX), the deepest depression in the Arctic ocean (5569 m depth); (4) HGIV, located in the center of the strait (2462 m depth); and (5) SVI, a station on the Svalbard shelf (272 m depth). Four McLane Large Volume Water Transfer Systems (WTS-LVs) were attached to a standard CTD wire to sample MP from within the near-surface (1−3 m), ∼300 m (250−308 m), ∼1000 m (974−1022 m), and above the seafloor (2449−5350 m) depth layers during CTD rosette casts (Table 1). After 1 h of filtration (218−561 L) through a stainless steel filter of 32 μm mesh size and 142 mm diameter (MP filter, Figure S1a) at the target depth layer, WTS-LVs were retrieved and MP filters stored in glass jars at −20 °C. A total of 18 MP filters were obtained. Samples for particulate organic carbon (POC), particulate organic nitrogen (PON), and total particulate matter (TPM) were taken by a rosette sampler equipped with SEA-BIRD CTD system and 24 Niskin bottles (12 L), with subsamples processed onboard (see Engel et al. (2019)[39] for details). A video-guided multiple corer (MUC; Oktopus GmbH) holding eight cores of 100 mm diameter was used to sample sediments and environmental parameters according to Bergmann et al. (2017)[2] at the same stations as the water samples were taken. The top 5 cm of three sediment cores taken at each station were sliced off with a metal spatula, wrapped into tin foil and stored at −20 °C.

Sample Purification and Microplastic Identification. MP filters were thawed, removed from the glass jars and placed into MP reactors. A MP reactor is a semienclosed unit, which contains stainless steel metal filters of 20 μm mesh size at both ends. This unit allows the addition and removal of solutions by vacuum and pressure filtration without sample transfer (Figure S1b, see Lorenz et al. (2019)[36] for the details of MP reactors). Glass jars were thoroughly rinsed with Milli-Q water and subsequently with 35% prefiltered ethanol into the reactors to wash off particles adhering to the inner surfaces of the jars. The samples were purified in the reactors by an enzymatic-oxidative treatment with sodium dodecyl sulfate (SDS), protease, cellulase, and hydrogen peroxide as described in Löder et al. (2017).[40] Visual inspection returned no particles >500 μm size on MP filters. After purification, the MP filters were taken out of the MP reactors and rinsed with Milli-Q water into the reactors (Figure S1c). Each MP filter was then inspected by stereomicroscope (Olympus SZX16) to ensure that no particles remained. Purified water samples were obtained by removing the filters from the bottom ends of the MP reactors and rinsing these into 100 mL glass bottles.[36]

Separation and size fractionation of the sediments were carried out as described in Bergmann et al. (2017).[2] Size fractionation resulted in particles of >500 μm size, which were manually sorted, inspected under a stereo microscope (Olympus SZX16, Olympus) at a 100−320× magnification and putative MPs identified using an attenuated total reflection (ATR, Paragraph S2) FTIR unit (Bruker Optik GmbH).[2] Before the purification of <500 μm size fraction, a comparison of enzymatic-oxidative (as used for water samples) and Fenton's reagent purification (as used in a previous study on Arctic sediments[2]) was performed on another set of Arctic sediments (Paragraph S3). The aim of this analysis was to assess if FTIR analyses of identical sediments, which have been purified with each of these two methods, result in different particle type and size measurements. Since this analysis did not reveal significant differences between methodologies, Fenton's reagent was selected to comply with the purification method of the earlier study of HAUSGARTEN sediments.[2]

Focal plane array (FPA) based FTIR imaging analysis was applied to measure the small size fraction (11−500 μm) of the water and sediment samples.[2,34,36,41] The mesh size of the MP filters (32 μm) and eventually also the filters of the MP reactors (20 μm) mark the lower size limit of the collected particles. However, MP incorporated aggregates within samples[30] and a decrease over time in fluid permeability during the filtering processes[42] may have led to a capture of yet smaller particles. Therefore, our measured concentrations of particles in 11, 25 (>11 ≤ 25 μm), and partly, 50 μm (>25 ≤ 50 μm) size classes are semiquantitative. An appropriate quantity of water and sediment subsamples was assessed by FlowCam (Fluid Imaging Technologies, Scarborough, USA)[2] to prevent filter overload.[36] Subsamples (Table 1) were concentrated on aluminum oxide filters (Ø = 25 mm; pore size, 0.2 μm; Anodisc, Whatman, Germany) (Figure S1d). These Anodisc filters (filter area = 184 mm^2, 77 × 77 FPA fields) were subsequently dried at 30 °C for 2 days and measured via FTIR imaging (Paragraph S4). Fiber detection[43] was not available at the time of analyses; therefore, fibers were excluded from the results as they were in comparable previous studies.[2,4,35,36,44]

Automated Analysis of FTIR Data. The measured FTIR data were analyzed via the automated analysis pipeline[34] excluding human bias. Within this process, each spectrum was compared twice against the reference database[45] using spectra correlation of the raw and the first derivative data. A spectrum is identified if both methods yield the same polymer type, and the result is transferred into an image. Particle numbers, polymer size classes, and types were obtained via image analysis using Python 3.4 scripts and Simple ITK functions (see Primpke et al. (2017)[34] for details).

Contamination Prevention. Water and sediment sampling equipment (tweezers, glass jars, spatula, ruler) were rinsed thoroughly with Milli-Q (0.22 μm filtered water, Millipore) before every deployment. MP filters were placed and retrieved with metal tweezers. Contamination prevention in the laboratory and creation of procedural blanks of sediment samples were conducted according to Lorenz et al. (2019).[36] Glass or metal equipment were used throughout, with the exceptions of tubing and seals (silicone), $ZnCl_2$ filters (polypropylene; pleated cartridge 37 filters) and squeeze bottles (polytetrafluorethylene). All chemicals were filtered before usage through 0.2 μm (GTTP, polycarbonate), enzymes and sodium dodecyl sulfate (SDS) over 0.45 μm (cellulose nitrate) or 1.2 μm (GF/F 40 glass fiber) filters to remove particles from the solutions. Dustboxes (DB1000, G4 prefiltration, HEPA-H14 final filtration, Q = 950 m^3/h, Möcklinghoff Lufttechnik) were placed at the sediment separation, purification and FTIR imaging laboratories to prevent contamination of the samples by airborne particles. The purification with the MP reactors and filtration of the samples were processed in a laminar flow cabinet (ScanLaf 43 Fortuna 1800, LaboGene, Lillerød, Denmark). A blank sample was taken on-board to assess the contamination during the deployments of WTS-LVs. A total of 100 L of prefiltered freshwater was pumped with a WTS-LV. Prefiltration was done

https://dx.doi.org/10.1021/acs.est.9b06981
Environ. Sci. Technol. 2020, 54, 4079−4090

by attaching a water filter with metal cartridges of 2−3 μm mesh to a freshwater source. The MP filter of the blank sample was purified and analyzed together with the water samples. MP amounts in the water samples were blank-corrected for contamination based on the result of the blank sample analysis and in the sediment samples based on the result of the procedural blank as described in Bergmann et al. (2017).[2] The contamination, which was caused by certain polymers during the sampling and analysis processes of the water samples, was eliminated from the results (Paragraph S5).

Particle Tracking. The origin of MP particles measured in the analyzed water samples was estimated with a Lagrangian particle-tracking algorithm, following the approach of Wekerle et al. (2018).[37] Backward three-dimensional (3D) trajectories of MP particles in the deep water column (300 m, 1000 m, above seafloor) were computed for four stations in the Fram Strait (EGIV, HGIV, HGIX, N5) with three different settling velocities. Particles were released once per day during 2016 at corresponding sampling station × depths and tracked backward in time until they reached the sea surface, where they may have commenced sinking (surface origin). Therefore, a reversed flow field was used, as if the particles were rising from the sampling depth to their surface origins via lateral displacement with a negative sinking and reversed horizontal velocity (vertical ocean velocities were neglected). Daily averaged horizontal velocity fields were taken from the Finite-Element Sea-Ice Ocean Model (FESOM, version 1.4). The model configuration used in this study was optimized for the Fram Strait region, applying a mesh resolution of 1 km in this area. It covers the time period 2010−2016, is forced with atmospheric reanalysis data from Era-interim, and is initialized with model fields from the simulation described in Wekerle et al. (2017).[46] A time step of 1 h was used for the trajectory calculations, yielding hourly positions and corresponding values of temperature and salinity. The sampling depths for HGIV above seafloor and SVI 300 m depth layers were not included in the computation since the analyses did not reveal MP particles in these water samples. Previous studies have shown that the settling velocities of marine particles are altered by a factor of −2.87 to 1.64 when MP is incorporated into them, suggesting a decrease in the settling velocity for most of the cases (between −2.87 and −1.35).[24−26] To account for this variability, a representative factor of −2.25 was selected from Cole et al. (2016)[25] and settling velocities used in Wekerle et al. (2018)[37] (20 m, 60 m d^{-1}, 120 m d^{-1}) were modified accordingly (9 m, 27 m d^{-1}, 53 m d^{-1}). These settling velocities match with the results of an earlier experimental study.[47]

In addition to the 3D particle trajectories described above, two-dimensional (2D) trajectories were computed for the MP particles in the near-surface water samples by using only the surface velocity field of the ocean model. This was done for all five stations (EGIV, HGIV, HGIX, N5, SVI). As in the case of the 3D trajectories, particles were released once per day throughout 2016 and tracked backward in time for 365 days. The computation was stopped earlier if the particle reached the coast. Probability maps of the particle distributions were generated by counting the visit of a particle as it crossed a bin and normalizing by the total number of particles (365).

Environmental Parameters. Temperature, salinity, and dissolved oxygen (O_2) data were obtained from synchronous CTD measurements.[48] Where no data were available for the same depth as at which the water column was sampled for MP, measurements from the nearest depths were included in the data sets (Table S6). Sea ice conditions at the surface were determined from daily concentrations of sea ice retrieved from Centre d'Exploitation et de Recherche SATellitaire (CERSAT; http://cersat.ifremer.fr/).[49] Ice coverages were calculated as the percentage of the days (for the near-surface depths and seafloor) and surface origins (for the deep water column) when sea ice concentration was >15% during the corresponding time period (2016 for the water column and 2000−2016 for the seafloor, see Paragraph S6 for details). POC and PON were analyzed as described in Engel et al. (2019)[39] by filtering aliquots of 1 to 6 L of seawater onto combusted GF/F filters and TPM as in Bodungen et al. (2013).[50] Values for environmental parameters in sediments (porosity, chlorophyll *a*, chloroplastic pigment equivalent, particulate organic carbon, and phospholipids) were obtained as outlined in Bergmann et al. (2017)[2] by subsampling additional cores with cutoff syringes of 2 cm diameter, which were analyzed at 1 cm intervals down to 5 cm sediment depth.

Design of Permutational Multivariate Analysis of Variance for the Analysis of Polymer Compositions. Multivariate analyses of polymer type and size class composition as concentrations (hereafter polymer composition, unless only type or size class composition is referred to) were performed using PRIMER-e version 6.1.16 with PERMANOVA 1.0.6.[51] A permutational multivariate analysis of variance (PERMANOVA) routine with 9999 permutations was carried out to assess differences between a priori groups of stations (EGIV, HGIV, HGIX, N5, SVI), depth layers (near-surface, 300 m, 1000 m, above seafloor, sediment), water masses (polar, Atlantic, deep waters), surface locations (N5 and EGIV, ice edge; HGIV and HGIX, center; SVI, shelf) and realms (water column and sediment). CTD profiles showed waters below 0 °C (polar waters) at the near-surface depth layers of the deep stations. Warm waters of Atlantic origin (>2 °C) prevailed at 300 m depth layers at all stations and at SVI. For data analyses, 1000 m and above seafloor layers were categorized as deep waters. Data treatment prior to PERMANOVAs was done based on the sampling realms (i.e., water column only or through the water column and sediment, see subsequent sections). Two-way PERMANOVAs were performed using station × depth layer (without interaction), station × water mass, and station × marine realm as fixed factors. Surface locations were compared one-way to evaluate the influence of ice coverage on MPs distribution. Furthermore, a canonical analysis of principal coordinates (CAP) was applied to analyze and visualize significant differences between the a priori defined groups. Temporal changes in MP concentrations and polymer type compositions of the sediments were investigated on the data set by including in the analysis results from a previous HAUSGARTEN study[2] in 2015, by running PERMANOVA on Bray−Curtis similarity matrix of square-root transformed data set of polymer type compositions. MP concentrations from two years were compared with one-way analysis of variance (ANOVA).

Analysis of the Microplastic Distribution in the Water Column. Univariate statistical analyses were performed with Sigmaplot 14.0 on water column MP concentrations. A Kolmogorov−Smirnov normality test failed for MP concentrations (K−S Dist. = 0.387, P = 0.037) because of the high MP abundance in the N5 near-surface sample. Therefore, this station was excluded from univariate analyses to achieve

https://dx.doi.org/10.1021/acs.est.9b06981
Environ. Sci. Technol. 2020, 54, 4079−4090

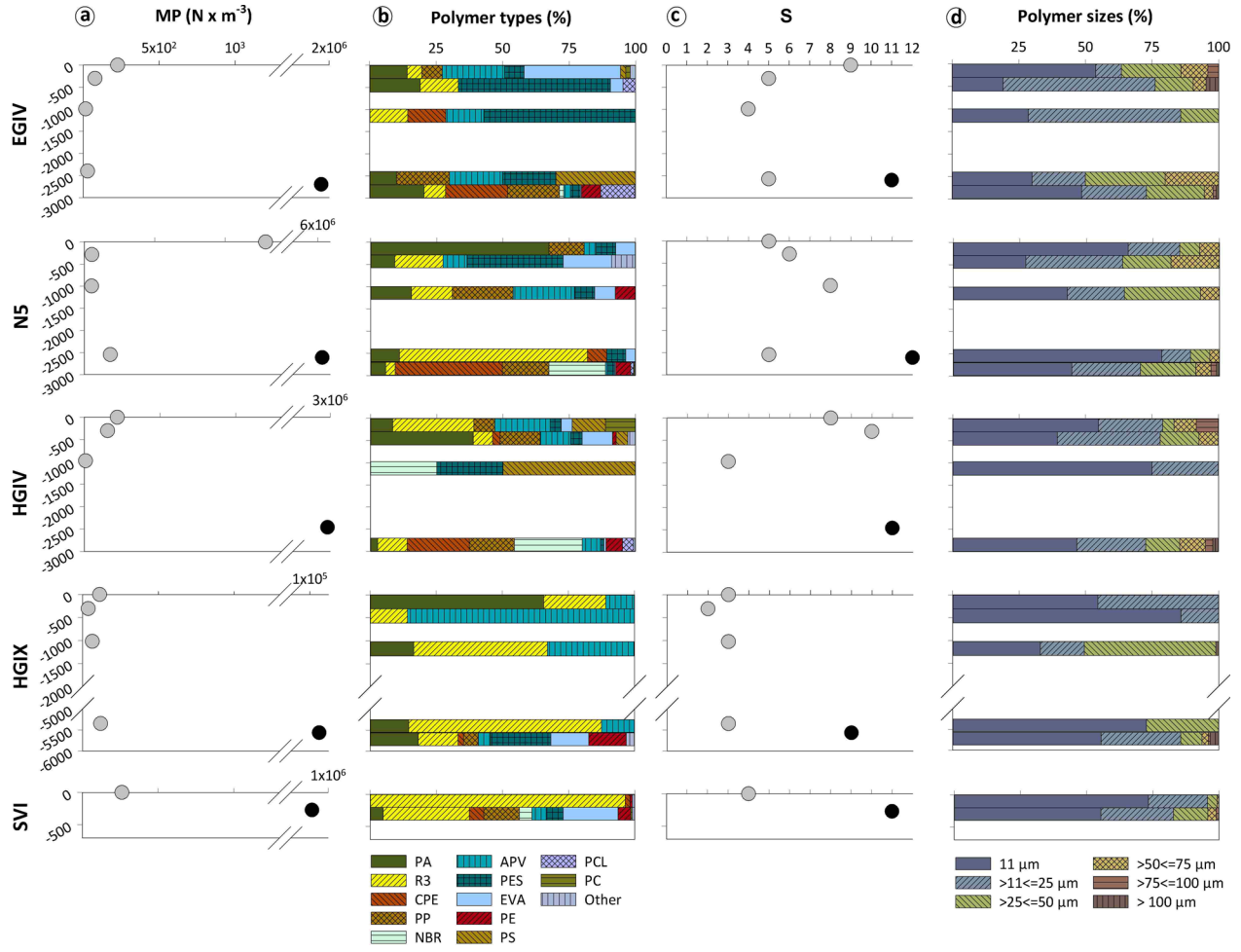

Figure 1. Microplastic concentrations, percentages of polymer types, total polymer counts, and percentages of polymer size classes of each sample. For visual purpose, the sampling depths of the above seafloor and sediment layers were adjusted to prevent the bars from overlapping. (a) MP concentrations. Gray dots represent MP concentrations in the water samples and black dots in the sediments. (b) Percentages of polymer types (PA, polyamide; R3, ethylene-propylene-diene rubber; CPE, polyethylene-chlorinated; PP, polypropylene; NBR, nitrile rubber; APV, acrylates/polyurethanes/varnish/lacquer; PES, polyester; EVA, ethylene-vinyl-acetate; PE, polyethylene; PS, polystyrene; PCL, polycaprolactone; PC, polycarbonate; other, polyvinylchloride, rubber type 1, polysulfone, cellulose acetate).[45] (c) Total polymer type counts (S) in the water and sediment samples. Gray dots represent S in the water samples and black dots in the sediments. (d) Percentages of polymer size classes.

normality (K−S Dist. = 0.168, $P > 0.2$) and mean MP concentrations were then calculated by excluding this sample. Stations, depth layers, water masses, and surface locations were compared with ANOVA followed by a Holm−Sidak test to assess differences between different groups. A Spearman rank order correlation was used to assess the relationships between MP concentrations and environmental parameters (sampling depth, temperature, salinity, O_2, ice coverage, POC, PON, TPM). A PERMANOVA routine was executed on a Bray−Curtis similarity matrix of square-root transformed data sets of polymer compositions. Polymer compositions of different stations, depths, water masses, and surface locations were compared. The similarity percentage (SIMPER) routine of PRIMER-e was performed to assess within group (stations, depth layers, water masses, surface locations) similarities and between group dissimilarities. The distance-based linear model (DistLM) routine of PRIMER-e was applied to investigate multivariate multiple regressions between polymer compositions and environmental parameters. Ice coverage, POC, PON, and TPM values were not obtained for all of the depth layers of HGIV, HGIX, and SVI. Therefore, three sample groups (1−3) of polymer compositions (Paragraph S7) were created for DistLM analyses based on the availability of these values. Marginal tests of the DistLM routine were run with 9999 permutations to assess the correlations between polymer compositions and each environmental parameter. The "Best" selection procedure with the "Akaike information criterion (AIC)" was used to find the regression models. Following the selection of the fitting model (Paragraph S7), the relations were visualized with distance-based redundancy analysis (dbRDA).

Analysis of the Microplastic Distribution through the Water Column and Sediment. The Hellinger dissimilarity measure is not sensitive to magnitude differences in abundances, and therefore, it was applied to square-root transformed standardized data sets of polymer compositions of water column and sediment in combination.[36] A PERMANOVA was applied to assess the differences in polymer compositions between stations, depths, marine realms, and station × marine realm interactions. Total polymer types (S) and Pielou's evenness (J') of polymer compositions were calculated to assess the diversity of polymer compositions since these two diversity measures are not based on abundances. PERMANOVA was run for stations, depth layers, and realms

https://dx.doi.org/10.1021/acs.est.9b06981
Environ. Sci. Technol. 2020, 54, 4079−4090

on Euclidean distances of log(x + 1) transformed diversity data set.

RESULTS

Between 218 and 561 L of water were filtered with large volume pumps. Depending on the particle load of each sample, 5−100% of the purified sampled volume were measured by FTIR imaging (Table 1). MPs were found in 16 out of 18 samples ranging from 9−1287 N m^{-3} (Figure 1a) with a mean concentration of 95 ± 85 N m^{-3} (±SD; 161 ± 293 N m^{-3}, if N5 near-surface concentration included). A total of 15 types of synthetic polymers in a size range of 11−150 μm were identified (Figure 1b). The highest mean MP concentration through the entire water column was detected at the coastal SVI (131 ± 185 N m^{-3}) and the lowest mean at the deep HGIX (84 ± 39 N m^{-3}). The highest mean concentration through the water column of the deep stations was found at N5 (98 ± 77 N m^{-3}, excluding near-surface concentration). ANOVA indicated no significant difference between stations (P > 0.050). Comparison of depth layers revealed a significant difference (ANOVA F = 5.97, df = 3, P = 0.009) caused by the disparity of samples taken near-surface and at 300 m (Holm−Sidak t = 3.41, P = 0.023) and between near-surface and 1000 m depth layers (Holm−Sidak t = 3.89, P = 0.011). No significant difference was found between water masses and different surface locations (P > 0.050).

The highest MP concentration within sediments was detected at N5 (13 331 N kg^{-1}) and the lowest at HGIX (239 N kg^{-1}) (Table 1); 4−52% of each purified sediment sample volume was measured by FTIR imaging, giving a mean concentration of 4730 ± 5107 N kg^{-1} (Figure 1a). A total of 12 polymer types in a size range of 11−200 μm were identified (Figure 1b and d). ANOVA showed no significant difference between samples from 2015 and 2016 (P > 0.050).

Polymer Types. Six polymer types accounted for 96% of all synthetic particles found in water samples (polyamide [PA], 39%; ethylene-propylene-diene rubber [R3], 23%; acrylates/polyurethanes/varnish/lacquer [APV], 10%; polypropylene [PP], 8%; polyester [PES], 8%; ethylene-vinyl-acetate [EVA], 8%) (Figure 1b, Table S4a). PERMANOVA of polymer types for station × depth groups revealed significant differences between stations (pseudo-F = 2.02, P(perm) = 0.017) but not between depth layers. The polymer composition at HGIX was significantly different from N5 (t = 2.31, P(perm) = 0.036) and the CAP routine revealed a similar result (Figure S8a). Analysis of station × water mass groups did not show any difference (P(perm) > 0.050). HGIX harbored only PA, APV, and R3 at all depth layers with a 66% within group similarity, whereas the within group similarity of the other stations ranged between 16% and 39%. The lowest dissimilarity between stations was observed between EGIV and N5 (57%), and the highest between EGIV and SVI (94%). Surface locations showed significant differences (pseudo-F = 1.83, P(perm) = 0.049), which was also confirmed by the CAP routine (Figure S8b). Polyethylene-chlorinated (CPE, 31%), nitrile rubber (NRB, 18%), and PP (17%) comprised the highest proportions in sediments, whereas other polymer types contributed 1−9%. There was no significant difference in polymer type compositions of sediments sampled in 2015[2] and 2016 (pseudo-F = 1.55, P(perm) = 0.140).

Data analyses on MP concentrations through the water column and sediment at stations and realms revealed significant differences between stations (for station × depth layer: pseudo-F = 1.73, P(perm) = 0.020) (Figure S8c) and realms (for station × realm: pseudo-F = 3.37, P(perm) = 0.003) (Figure S8e). Polymer type compositions at HGIX were significantly different from N5 (pseudo-F = 1.94, P(perm) = 0.039). Polymer diversity was higher in sediment samples compared to water samples (Figure 1c). PERMANOVA results of diversity indices (S and J') for station × depth layer showed significant differences between depth layers (pseudo-F = 3.12, P(perm) = 0.011) because of the differences between sediment and 1000 m (pseudo-F = 4.79, P(perm) = 0.014) and sediment and above seafloor layers (pseudo-F = 3.49, P(perm) = 0.038). Water column and sediment diversity indices (S and J') between stations and realms were significantly different (station pseudo-F = 2.31, P(perm) = 0.0002; realm pseudo-F = 13.93, P(perm) = 0.039, respectively).

Polymer Size Classes. There were no significant differences in the polymer size composition between stations, realms, depth layers, water masses, station × water mass interactions, and surface locations, but diversity indices between realms were significantly different for station × realm groups (pseudo-F = 11.12, P(perm) = 0.0013). The largest MP particle found within the water column was in the 150 μm size class (>125 ≤ 150 μm, Table S4b). Twenty-three putative MP particles >500 μm including 14 fibers (Table S2 and Figure S2) were detected in the sediment samples. The measurements by ATR-FTIR did not reach hit quality above 700 in repeated measurements (Table S2). Therefore, they were not included in the data analyses. The largest MP particle detected by FTIR imaging was in the 200 μm size class (>175 ≤ 200 μm, Table S4b). MP of 11−25 μm size classes accounted for 82% of the synthetic particles (Figure 1d and Table S4b) in the water column and 72% in the sediment. Only 0.15% of the particles exceeded 100 μm in the water column and 1% in the sediment.

Environmental Parameters. MP concentrations in the water column were positively correlated with POC (Spearman ρ = 0.66, P = 0.01), PON (ρ = 0.60, P = 0.022), TPM (ρ = 0.61, P = 0.025), sampling depth (ρ = 0.48, P = 0.045), O_2 (ρ = 0.53, P = 0.025). Marginal tests of polymer size compositions showed statistically significant values for sampling depth, O_2 (for sample groups 1−3), POC (for sample groups 2, 3), PON (for sample group 2), and TPM (for sample group 3) (Table S7b). The multicollinearity among sampling depth, O_2, POC, PON, and TPM (Table S7c) was taken into account during the selection of multivariate multiple regression model selection (Paragraph S7). Marginal tests of polymer types showed significant values for sampling depth, O_2 and TPM only for sample group 3 (Table S7b). Considering the multicollinearity among O_2, POC, PON, TPM, as well as the significant correlation between polymer compositions and these parameters, any of them (or in combination) would explain the modeled variation among the samples. For the polymer size compositions, the multivariate regression models of O_2 and salinity were selected as the distance-based linear models for the sample groups 1 and 2 (Figure S7a, R^2 = 0.30, AIC = 110, and Figure S7b, R^2 = 0.41, AIC = 88, respectively). If environmental parameters including TPM were examined (sample group 3), the models of sampling depth and TPM were selected for polymer size and type compositions (Figure S7c, R^2 = 0.27, AIC = 92 and Figure S7d, R^2 = 0.47, AIC = 81, respectively). MP concentrations in sediments were not correlated with environmental parameters.

https://dx.doi.org/10.1021/acs.est.9b06981
Environ. Sci. Technol. 2020, 54, 4079−4090

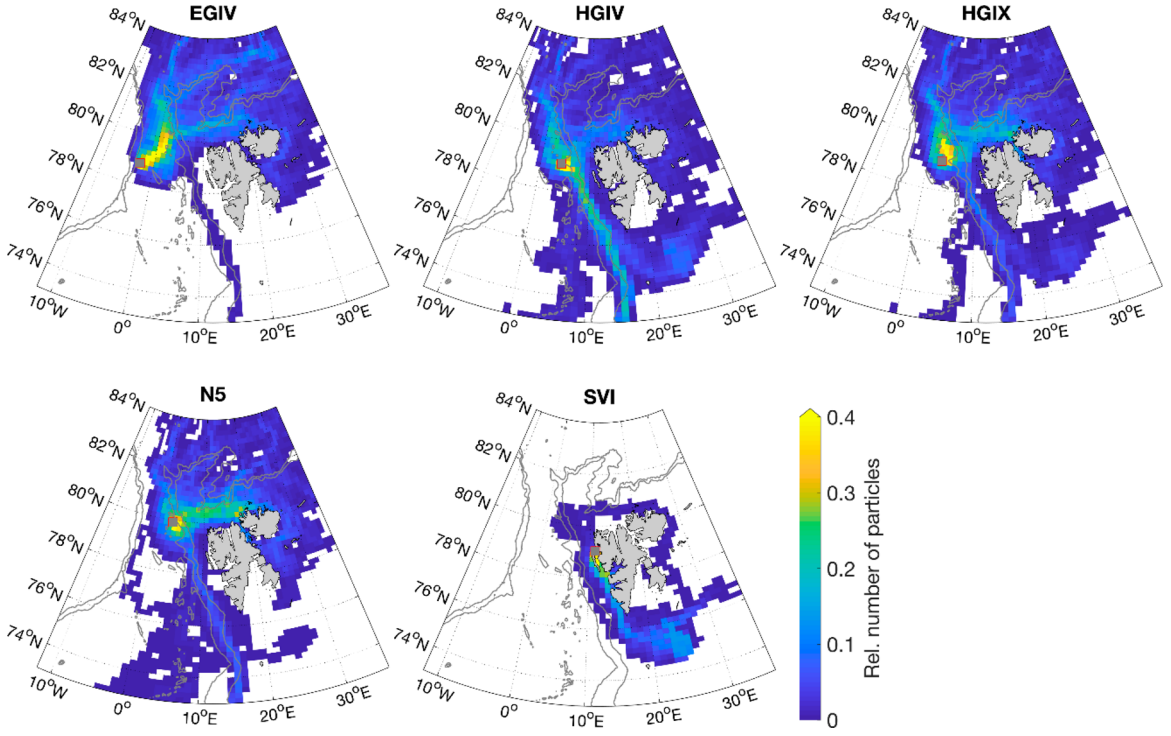

Figure 2. Source areas of MP particles detected at the near-surface depth layers at five stations (gray dots) of the HAUSGARTEN Observatory as computed by 2D backward trajectories, using the surface velocity field of the ocean model. The color scale shows the relative number of particles that crossed a grid box. The gray lines represent the topography at 1000 and 2000 m depths.

Particle Tracking. 2D trajectories showed distinct patterns of source areas of the MP particles in the near-surface samples (Figure 2). An area to the south of Svalbard was exclusively projected as the source area of particles arriving at SVI, which were carried by the Svalbard Coastal Current. At EGIV, the trajectories suggested a pathway from the North to the sampling station. Particles at HGIV were estimated to originate from an area to the south of the Fram Strait carried by the WSC. By contrast, the majority of the particles arriving at N5 and HGIX were projected to be carried from north of Svalbard.

A total of 11 groups of 3D trajectories were obtained for the MP particles in the deep water column samples (300 m, 1000 m, above seafloor) (Figure S9). A total of 12 045 surface origin points were computed, and a summary data set was created (Table S9). 3D trajectories revealed the WSC and EGC as the prime vector for particle transport to HGIV, N5, and HGIX, yet with different intensities. The slower the settling velocity the larger were the catchment areas. Most of the particles detected at EGIV originated from the sea-ice covered areas (66%) and thus from polar waters and at HGIV from Atlantic waters (73%). Particles at HGIX originated from both water masses: 52% from polar waters and 48% from Atlantic waters. For all stations, 3D trajectories revealed mostly south of the Fram Strait as the source area of the particles settling with a velocity of 9 m d^{-1}.

DISCUSSION

Our results show that MP particles are present throughout the Arctic water column (9−1287 N m^{-3}). Even though MP concentrations in water samples were not as high as in sediments (present study, 239−13 331 N kg^{-1}; earlier study,[2] 42−6595 N kg^{-1}) and in sea ice (1100−12 000 N L^{-1}),[4] it should be noted that water samples represent a snapshot in time, whereas sediment and sea ice samples reflect MP accumulation over longer time scales. The mesh size of the sampling and processing filters most likely resulted in the loss of smaller particles (<32 and <20 μm, respectively). Therefore, MP concentrations of the 11, 25, and partly 50 μm size classes have to be considered as semiquantitative, indicating that a more abundant number of particles in the small size range of MP may be present as pollution in the Arctic. The fact that sediments harbored 16×10^3 times higher quantities than were observed in the water column further proves that the Arctic seafloor constitutes a long-term sink for MP.[2,52] This was corroborated by a higher polymer diversity being found in the sediments than in the water column, which indicates the accumulation of a higher variety of polymers over long time scales. There is currently no standard operational procedure with respect to sampling, analysis, and reporting of MP concentrations, but the number of MP per unit volume is the most common unit used for water samples.[2,53] A conversion of quantities to cubic meters may result in extrapolation of MP counts, yet such a conversion is necessary to allow comparisons between studies. The large-volume pumps used in the current study filtered between 218 and 561 L of seawater per sample, resulting in a similar or lower magnitude of extrapolation when compared to the earlier deep water column studies[18,20,21] (except Choy et al. (2019)[19]). For some samples, particle concentrations within the purified volume were high, and care had to be taken to ensure that Anodisc filters were not overloaded. Thus, for example, only 5% of the near-surface sample of the northern station could be analyzed, which showed the highest MP concentration of all water samples (1287 N m^{-3}). While this value was treated as an outlier in univariate analyses, the high abundance did not come as a surprise as this station is located closest to the marginal ice zone. Indeed, globally, some of the highest MP concentrations

https://dx.doi.org/10.1021/acs.est.9b06981
Environ. Sci. Technol. 2020, 54, 4079−4090

have been found in Arctic sea ice.[4,5] Furthermore, the highest MP concentration among above seafloor samples and in HAUSGARTEN sediments (from surveys in 2015[2] and 2016) was found at the northern station.

Combining results from sediments with those from water samples provided more insight into accumulation mechanisms of MP particles. However, different sampling realms, methods and large discrepancies in concentrations constrain the assessment of MP distribution throughout these ecosystem compartments. As samples from Arctic waters have not been analyzed with our methods before, the concentrations in the water column were completely unknown, and the samples were purified following enzymatic-oxidative treatment, the efficiency of which was proven for several environmental matrices.[36] On the other hand, our sediment samples were a part of a time-series of the HAUSGARTEN observatory, with samples purified with Fenton's reagent. Therefore, Fenton's reagent was used for the purification of the sediment samples to maintain the consistency of the time series since the comparison of the two treatments did not show any difference in polymer compositions. Most previous studies on MP in Arctic sediments[54,55] have relied on visual selection of putative particles, which were verified by FTIR (except earlier study of HAUSGARTEN[2]). Indeed, HAUSGARTEN sediments seem to harbor many more MP particles (239−13 331 N kg^{-1}) compared to other Arctic locations (5−69 N kg^{-1}),[54] but if we limit the comparison to the >100 μm size range, MP concentrations at HAUSGARTEN are in a similar magnitude (8−142 N kg^{-1}). However, if fibers are excluded, which account for 64% of the MP particles at other Arctic locations,[54] HAUSGARTEN sediments show substantially higher MP concentrations.

MPs from near-surface layers have been reported from Antarctica[56] (0.17 N m^{-3}), NE Pacific[57] (8−9,180 N m^{-3}), Monterey Bay[19] (2,900 N m^{-3}), European coasts[58] (~300 N m^{-3}), and North Atlantic Subtropical Gyre[58] (~100 N m^{-3}). The latter two are pertinent to compare with the HAUSGARTEN observatory results directly as Enders et al. (2015)[58] identified MPs down to 7 μm. Near-surface concentrations at HAUSGARTEN appear higher (113−1287 N m^{-3}) than measured in the North Atlantic Subtropical Gyre.[58] Levels of 0−31 N m^{-3} with fibers (except Morgana et al. (2018)[59]) accounting for 91−96% were reported from the near-surface layers of the Arctic Ocean.[18,59−61] Only one of the near-surface samples contained MP particles >100 μm at HAUSGARTEN. Overall, 99.9% of MPs in the water column were between 10 and 100 μm, highlighting once more[2,4,8,35,36] how crucial it is to detect small MP particles (<100 μm) to quantify the true extent of MP pollution in the environment. There may well be high abundances of yet smaller MP particles below our current detection limit (11 μm). This is important because such information affects the outcome of risk assessments.[62] A higher contribution of particles >100 μm in the sediment compared to the water column indicates a lower residence time of small MP in surface waters, which contradicts earlier studies.[58,63] Whether this inconsistency is due to hitherto unnoticed amounts of small MP or due to possible interactions with water column processes is an important research question.

The highest MP concentrations were found in the near-surface samples from all stations, except for the Molloy Deep. While increasing concentrations with depth were reported from the Mariana Trench (2060−13 510 N m^{-3}),[20] no clear pattern was found at the Arctic Central Basin (0−375 N m^{-3})[18] and highest concentrations were observed between 200 and 600 m at Monterey Bay (15 000 N m^{-3}).[19] In the present study, the mean MP concentration decreased 6-fold toward the 1000 m depth layer resulting in profiles similar to those of POC,[39] with concentrations doubling above the seafloor. Interestingly, the vertical distribution of particles at the Molloy Deep indicated a different mechanism in the MP flux, which implies the importance of the local ocean circulation for the distribution of MP. A similar polymer type composition was found at all depths of the Molloy Deep, whereas at the other stations polymer diversity varied between depth layers. Additionally, the Molloy Deep is the only station where no positively buoyant polymers were found and where the highest MP concentration among different sampling depths occurred at the closest sampling location to the seafloor. The Molloy Deep is the deepest known depression in the Arctic Ocean, which acts like a trap for organic matter because of its depth, topography, and hydrography.[64] Model studies indicated that one of the two main recirculation branches of the WSC cyclonically encircles the Molloy Deep.[46,65] As in the case of eddies, the cyclonic loop leads to upwelling at its center and divergence of particles at the surface.[66] The higher MP concentration above the seafloor, in contrast, might be related to the steep slopes around the Molloy Deep, which may facilitate accumulation of particles toward nepheloid layer. Even though the full depth of this station is twice the depth of most of the other HAUSGARTEN stations, 3D trajectories showed a catchment area identical to other stations.

The positive correlation between MP concentrations and O_2, POC, PON, and TPM in the HAUSGARTEN water column is remarkable. Correlations alone may not be sufficient to draw firm conclusions, but earlier studies have already shown that MP particles incorporate into marine snow,[22,23] fecal pellets,[24,25] and phytoplankton heteroaggregates[26−29] indicating biological pathways in the downward flux of MP particles. Zhao et al. (2018)[30] identified MP in 73% of the marine aggregates collected during field surveys and proposed that they act as a transport medium for MP in the water column. Despite the 32 μm mesh size of the sampling filters used, the detection of particles <32 μm in the HAUSGARTEN water column corroborates these findings. The occurrence of MP particles in phytoplankton heteroaggregates is interesting in the context of the Arctic Ocean since the POC concentration in the upper water column of the Fram Strait is strongly related to phytoplankton growth.[39] Processes related to sea ice are driving factors for the biological pump in the Arctic Ocean.[67] Sea-ice-derived cryogenic gypsum enhances carbon export during under-ice blooms of the haptophyte *Phaeocystis*.[68] Such ballasting effects may also enhance the flux of MP to the deep ocean. Interannual variability affects MP amounts in aquatic environments.[69] The sampling at the HAUSGARTEN observatory was carried out in June−July, during a period of phytoplankton blooms, which may have led to the correlation of MP with POC.

Earlier studies used MP fragments and beads in a range of 2−500 μm[22,24,26,70] to experimentally investigate whether they incorporate into marine particles or not. However, there are currently no data available as to how the size of MP affects the rate of this incorporation since experimental studies have investigated specific concentrations, polymer types, or sizes.[22,24,26,70] The distribution of MP size classes at HAUSGARTEN did not show any difference throughout the

https://dx.doi.org/10.1021/acs.est.9b06981
Environ. Sci. Technol. 2020, 54, 4079−4090

water column, which concurs with the particle and plankton size distribution from the upper water column in the Fram Strait.[71] Multivariate correlation between MP size classes and POC indicates size-related interactions of MP particles with biological processes. MP particles have been detected in larvaceans from 200 to 400 m depth[19,72] and in zooplankton.[24,70] Another Arctic-specific example is the ingestion of MP by polar cod (*Boreogadus saida*),[6,59] which is considered a keystone species and whose juveniles are particularly dependent on sea ice. Thus, another understudied mechanism of downward flux of MP particles may be the transportation by pelagic organisms through the water column. Small MP particles have been shown to decrease the survival and reproduction of the rotifer *Brachionus plicatilis*.[73] Along with the finding of almost all MP particles in the water column being <100 μm, these other observations also validate the concerns as to how much MP enters into the food chain and what effects this may have on the well-being of organisms, including humans.

Considering the complex hydrographic structure of the Fram Strait, it is crucial to adopt a holistic approach in the efforts of identifying sources, pathways, and sinks of MP. A validated model simulation[37] was used in the present study to track MP particles in the water column back to their potential source areas at the ocean surface. 3D particle trajectories emphasized the importance of lateral advection and variable particle settling velocities in the vertical distribution of MP particles. The vertical ocean velocities were neglected and a constant sinking speed was used in the model, which may be a particularly important parameter at frontal regions, and thus, they need to be investigated in future simulation efforts. It was estimated that MP particles detected above the seafloor traveled distances between 604 and 654 km. Therefore, when considering the sinking of MP particles, the focus should be rather on downward flux mechanisms than direct vertical transport. With the slowest settling velocity of 9 m d^{-1}, particles are exposed to the currents to a greater extent, and thus the influence of the WSC and of its recirculating branch, present at the surface and at intermediate depths of all deep stations, is much higher. Correspondingly, 3D trajectories suggested that most of these particles were carried to the Fram Strait from the south, which may be a pathway for positively buoyant polymers.

2D particle trajectories validated distinct spatial patterns in the transport of certain polymers. Ethylene-propylene-diene rubber was abundant in almost all water column samples and made up 96% of all the MPs detected at the surface layer of the Svalbard shelf station. 2D trajectories revealed south of Svalbard and the Barents Sea as the only source of these particles, suggesting North Atlantic and European origins. Ethylene-propylene-diene rubber is widely used in roofs, the automotive industry (as sealing material) and for artificial turf filling.[12] The latter is notable since it is widely used and poses a risk for human health.[12] Another distinct pattern was noticed in the near-surface samples of the station located in the East Greenland Current region. This layer contained the highest proportion of ethylene vinyl acetate (36%) among all samples and the modeled trajectories indicated polar waters as the only likely origin. This material is widely used in products, such as paints, coatings, safety glass, packaging, adhesives, and textiles.[74] This polymer accounted for up to 10% of the MP particles identified in an ice core from East Greenland[4] corroborating a sea ice origin. 3D trajectories also suggested a sea ice origin for the majority of the particles found in the deep waters of East Greenland. Polyamide dominated all water column samples and has been observed in Arctic sediments,[2] ice cores,[4,5] and snow[8] albeit in lower proportions. It is widely used in synthetic fabrics, carpets, sails, and fishing nets and is one of the dominant polymers used in European fisheries.[75] Because of its widespread usage, it is impossible to draw firm conclusions as to exact origins and transportation pathways of the polyamide particles observed in the current study. It may be speculated that increased fishery activity, an indirect consequence of the declining sea ice, may be a source for polyamide in Fram Strait waters. Acrylates/polyurethanes/varnish/lacquer, one of the most abundant polymers in the water column, is widely used as coating material in architectural, automotive, shipping, and wind turbine applications to protect or decorate surfaces.[74] It has also been a dominant polymer found in snow and ice cores.[4,8] Sea ice trajectories revealed the Laptev Sea as the potential origin of such material in one of the ice cores with a high abundance.[4]

Our data indicate a widespread MP pollution of the Arctic Ocean and support the hypotheses that the Arctic is an accumulation area for MP particles transported (i) from the North Atlantic via the thermohaline circulation,[76] (ii) from the north of the Fram Strait entrained in sea ice and released during melting,[4] (iii) from the Barents Sea,[77] (iv) via local emissions from increasing shipping activities,[15] (v) from different directions through the atmosphere and precipitation,[6] and (vi) from the discharge of rivers.[78] The findings from the Molloy Deep highlight the importance of local circulation features for the distribution of MP particles. Size-dependent relations between MP and biogenic particles suggest that biotic processes throughout the water column affect MP distribution. The POC flux to the Arctic seafloor is low;[79] however, sea ice decline in the Arctic and longer summer periods stimulate primary production.[80,81] It is unclear how incorporation of MP into marine aggregates affects the efficiency of the biological pump and consequently deep-sea ecosystem functions in the Arctic. Nevertheless, increasing plastic leakage into our oceans,[82] especially into an ecosystem which has already been stressed by climate change as the Arctic Ocean, may well have unknown ecological repercussions.

■ ASSOCIATED CONTENT

Supporting Information

The Supporting Information is available free of charge at https://pubs.acs.org/doi/10.1021/acs.est.9b06981.

Processing of the water column samples, identification of particles >500 μm by attenuated total reflection (ATR) FTIR unit, comparison of the purification methods, FTIR measurements, contamination elimination, environmental parameters in the water column and sediments, relationships between polymer compositions and environmental parameters in the water column, CAP of polymer type compositions, and simulation of the 3D backward particle trajectories (PDF)

■ AUTHOR INFORMATION

Corresponding Author

Mine B. Tekman − *Alfred-Wegener-Institut, Helmholtz-Zentrum für Polar- und Meeresforschung, 27570 Bremerhaven, Germany;* orcid.org/0000-0002-6915-0176; Email: mtekman@awi.de

https://dx.doi.org/10.1021/acs.est.9b06981
Environ. Sci. Technol. 2020, 54, 4079−4090

Authors

Claudia Wekerle − *Alfred-Wegener-Institut, Helmholtz-Zentrum für Polar- und Meeresforschung, 27570 Bremerhaven, Germany*

Claudia Lorenz − *Alfred-Wegener-Institut, Helmholtz-Zentrum für Polar- und Meeresforschung, 27570 Bremerhaven, Germany;* orcid.org/0000-0002-7898-7728

Sebastian Primpke − *Alfred-Wegener-Institut, Helmholtz-Zentrum für Polar- und Meeresforschung, 27570 Bremerhaven, Germany;* orcid.org/0000-0001-7633-8524

Christiane Hasemann − *Alfred-Wegener-Institut, Helmholtz-Zentrum für Polar- und Meeresforschung, 27570 Bremerhaven, Germany*

Gunnar Gerdts − *Alfred-Wegener-Institut, Helmholtz-Zentrum für Polar- und Meeresforschung, 27570 Bremerhaven, Germany*

Melanie Bergmann − *Alfred-Wegener-Institut, Helmholtz-Zentrum für Polar- und Meeresforschung, 27570 Bremerhaven, Germany;* orcid.org/0000-0001-5212-9808

Complete contact information is available at: https://pubs.acs.org/10.1021/acs.est.9b06981

Notes

The authors declare no competing financial interest.

■ ACKNOWLEDGMENTS

We thank the officers and crew of *RV Polarstern* and chief scientist of expedition PS99.2, T. Soltwedel. I. Schewe operated the multiple corer. S. Tippenhauer and S. Torres-Valdes operated the CTD. We thank G. Wegener, MPI, and MARUM for lending the pumps and S. Becker and J. Rapp for assistance with pump operations. N. Knüppel sampled and analyzed POC, POC, and TPM, E-M. Nöthig provided the dataset and gave advice on water-column processes along with M. Iversen. A. Purser helped with the language and graphical abstract. C. Peter helped with the assessment of the data in LITTERBASE. This work contributes to the Pollution Observatory of the Helmholtz-funded infrastructure program FRAM (Frontiers in Arctic Marine Research), which funded MBT and CW. The German Federal Ministry of Education and Research (Project BASEMAN—Defining the baselines and standards for microplastics analyses in European waters; BMBF Grant 03F0734A) funded G.G. and S.P. C.L. was funded by a Ph.D. scholarship of the Deutsche Bundesstiftung Umwelt (DBU), and M.B. and C.H. were funded by the Helmholtz-Gemeinschaft Deutscher Forschungszentren.

■ REFERENCES

(1) Borrelle, S. B.; Rochman, C. M.; Liboiron, M.; Bond, A. L.; Lusher, A.; Bradshaw, H.; Provencher, J. F. Opinion: Why we need an international agreement on marine plastic pollution. *Proc. Natl. Acad. Sci. U. S. A.* **2017**, *114* (38), 9994.

(2) Bergmann, M.; Tekman, M. B.; Gutow, L. Sea change for plastic pollution. *Nature* **2017**, *544*, 297.

(3) Law, K. L.; Morét-Ferguson, S. E.; Goodwin, D. S.; Zettler, E. R.; DeForce, E.; Kukulka, T.; Proskurowski, G. Distribution of Surface Plastic Debris in the Eastern Pacific Ocean from an 11-Year Data Set. *Environ. Sci. Technol.* **2014**, *48* (9), 4732−4738.

(4) Peeken, I.; Primpke, S.; Beyer, B.; Gütermann, J.; Katlein, C.; Krumpen, T.; Bergmann, M.; Hehemann, L.; Gerdts, G. Arctic sea ice is an important temporal sink and means of transport for microplastic. *Nat. Commun.* **2018**, *9*, 1505.

(5) Obbard, R. W.; Sadri, S.; Wong, Y. Q.; Khitun, A. A.; Baker, I.; Thompson, R. C. Global warming releases microplastic legacy frozen in Arctic Sea ice. *Earth's Future* **2014**, *2* (6), 315−320.

(6) Kühn, S.; Schaafsma, F. L.; van Werven, B.; Flores, H.; Bergmann, M.; Egelkraut-Holtus, M.; Tekman, M. B.; van Franeker, J. A. Plastic ingestion by juvenile polar cod (*Boreogadus saida*) in the Arctic Ocean. *Polar Biol.* **2018**, *41* (6), 1269−1278.

(7) Allen, S.; Allen, D.; Phoenix, V. R.; Le Roux, G.; Durántez Jiménez, P.; Simonneau, A.; Binet, S.; Galop, D. Atmospheric transport and deposition of microplastics in a remote mountain catchment. *Nat. Geosci.* **2019**, *12* (5), 339−344.

(8) Bergmann, M.; Mützel, S.; Primpke, S.; Tekman, M. B.; Trachsel, J.; Gerdts, G. White and wonderful? Microplastics prevail in snow from the Alps to the Arctic. *Science Advances* **2019**, *5* (8), eaax1157.

(9) Schmidt, C.; Krauth, T.; Wagner, S. Export of Plastic Debris by Rivers into the Sea. *Environ. Sci. Technol.* **2017**, *51* (21), 12246−12253.

(10) Qi, R.; Jones, D. L.; Li, Z.; Liu, Q.; Yan, C. Behavior of microplastics and plastic film residues in the soil environment: A critical review. *Sci. Total Environ.* **2020**, *703*, 134722.

(11) Wright, S. L.; Thompson, R. C.; Galloway, T. S. The physical impacts of microplastics on marine organisms: A review. *Environ. Pollut.* **2013**, *178*, 483−492.

(12) Kim, S.; Yang, J.-Y.; Kim, H.-H.; Yeo, I.-Y.; Shin, D.-C.; Lim, Y.-W. Health risk assessment of lead ingestion exposure by particle sizes in crumb rubber on artificial turf considering bioavailability. *Environ. Health Toxicol* **2012**, *27*, e2012005−e2012005.

(13) Lu, L.; Wan, Z.; Luo, T.; Fu, Z.; Jin, Y. Polystyrene microplastics induce gut microbiota dysbiosis and hepatic lipid metabolism disorder in mice. *Sci. Total Environ.* **2018**, *631*−*632*, 449−458.

(14) Jin, Y.; Xia, J.; Pan, Z.; Yang, J.; Wang, W.; Fu, Z. Polystyrene microplastics induce microbiota dysbiosis and inflammation in the gut of adult zebrafish. *Environ. Pollut.* **2018**, *235*, 322−329.

(15) Tekman, M. B.; Krumpen, T.; Bergmann, M. Marine litter on deep Arctic seafloor continues to increase and spreads to the North at the HAUSGARTEN observatory. *Deep Sea Res., Part I* **2017**, *120*, 88−99.

(16) Bergmann, M.; Klages, M. Increase of litter at the Arctic deep-sea observatory HAUSGARTEN. *Mar. Pollut. Bull.* **2012**, *64* (12), 2734−2741.

(17) Peeken, I.; Bergmann, M.; Gerdts, G.; Katlein, C.; Krumpen, T.; Primpke, S.; Tekman, M. B. Microplastics in the Marine Realms of the Arctic with Special Emphasis on Sea Ice. In *Arctic Report Card 2018*; 2018.

(18) Kanhai, L. D. K.; Gårdfeldt, K.; Lyashevska, O.; Hassellöv, M.; Thompson, R. C.; O'Connor, I. Microplastics in sub-surface waters of the Arctic Central Basin. *Mar. Pollut. Bull.* **2018**, *130*, 8−18.

(19) Choy, C. A.; Robison, B. H.; Gagne, T. O.; Erwin, B.; Firl, E.; Halden, R. U.; Hamilton, J. A.; Katija, K.; Lisin, S. E.; Rolsky, C.; Van Houtan, K. S. The vertical distribution and biological transport of marine microplastics across the epipelagic and mesopelagic water column. *Sci. Rep.* **2019**, *9* (1), 7843.

(20) Peng, X.; Chen, M.; Chen, S.; Dasgupta, S.; Xu, H.; Ta, K.; Du, M.; Li, J.; Guo, Z.; Bai, S. Microplastics contaminate the deepest part of the world's ocean. *Geochemical Perspectives Letters* **2018**, *9*, 1−5.

(21) Courtene-Jones, W.; Quinn, B.; Gary, S. F.; Mogg, A. O. M.; Narayanaswamy, B. E. Microplastic pollution identified in deep-sea water and ingested by benthic invertebrates in the Rockall Trough. *Environ. Pollut.* **2017**, *231*, 271−280.

(22) Porter, A.; Lyons, B. P.; Galloway, T. S.; Lewis, C. Role of Marine Snows in Microplastic Fate and Bioavailability. *Environ. Sci. Technol.* **2018**, *52* (12), 7111−7119.

(23) Zhao, S.; Danley, M.; Ward, J. E.; Li, D.; Mincer, T. J. An approach for extraction, characterization and quantitation of micro-plastic in natural marine snow using Raman microscopy. *Anal. Methods* **2017**, *9* (9), 1470−1478.

(24) Wieczorek, A. M.; Croot, P. L.; Lombard, F.; Sheahan, J. N.; Doyle, T. K. Microplastic Ingestion by Gelatinous Zooplankton May Lower Efficiency of the Biological Pump. *Environ. Sci. Technol.* **2019**, *53* (9), 5387−5395.

(25) Cole, M.; Lindeque, P. K.; Fileman, E.; Clark, J.; Lewis, C.; Halsband, C.; Galloway, T. S. Microplastics Alter the Properties and Sinking Rates of Zooplankton Faecal Pellets. *Environ. Sci. Technol.* **2016**, *50* (6), 3239−3246.
(26) Long, M.; Moriceau, B.; Gallinari, M.; Lambert, C.; Huvet, A.; Raffray, J.; Soudant, P. Interactions between microplastics and phytoplankton aggregates: Impact on their respective fates. *Mar. Chem.* **2015**, *175*, 39−46.
(27) Mao, Y.; Ai, H.; Chen, Y.; Zhang, Z.; Zeng, P.; Kang, L.; Li, W.; Gu, W.; He, Q.; Li, H. Phytoplankton response to polystyrene microplastics: Perspective from an entire growth period. *Chemosphere* **2018**, *208*, 59−68.
(28) Möhlenkamp, P.; Purser, A.; Thomsen, L. Plastic microbeads from cosmetic products: an experimental study of their hydrodynamic behaviour, vertical transport and resuspension in phytoplankton and sediment aggregates. *Elem Sci. Anth* **2018**, *6* (1), 61.
(29) Long, M.; Paul-Pont, I.; Hégaret, H.; Moriceau, B.; Lambert, C.; Huvet, A.; Soudant, P. Interactions between polystyrene microplastics and marine phytoplankton lead to species-specific hetero-aggregation. *Environ. Pollut.* **2017**, *228*, 454−463.
(30) Zhao, S.; Ward, J. E.; Danley, M.; Mincer, T. J. Field-Based Evidence for Microplastic in Marine Aggregates and Mussels: Implications for Trophic Transfer. *Environ. Sci. Technol.* **2018**, *52* (19), 11038−11048.
(31) Turner, J. T. Zooplankton fecal pellets, marine snow, phytodetritus and the ocean's biological pump. *Prog. Oceanogr.* **2015**, *130*, 205−248.
(32) Iversen, M. H.; Ploug, H. Ballast minerals and the sinking carbon flux in the ocean: carbon-specific respiration rates and sinking velocity of marine snow aggregates. *Biogeosciences* **2010**, *7* (9), 2613−2624.
(33) Setälä, O.; Fleming-Lehtinen, V.; Lehtiniemi, M. Ingestion and transfer of microplastics in the planktonic food web. *Environ. Pollut.* **2014**, *185*, 77−83.
(34) Bergmann, M.; Wirzberger, V.; Krumpen, T.; Lorenz, C.; Primpke, S.; Tekman, M. B.; Gerdts, G. High Quantities of Microplastic in Arctic Deep-Sea Sediments from the HAUSGARTEN Observatory. *Environ. Sci. Technol.* **2017**, *51* (19), 11000−11010.
(35) Haave, M.; Lorenz, C.; Primpke, S.; Gerdts, G. Different stories told by small and large microplastics in sediment - first report of microplastic concentrations in an urban recipient in Norway. *Mar. Pollut. Bull.* **2019**, *141*, 501−513.
(36) Lorenz, C.; Roscher, L.; Meyer, M. S.; Hildebrandt, L.; Prume, J.; Löder, M. G. J.; Primpke, S.; Gerdts, G. Spatial distribution of microplastics in sediments and surface waters of the southern North Sea. *Environ. Pollut.* **2019**, *252*, 1719−1729.
(37) Wekerle, C.; Krumpen, T.; Dinter, T.; von Appen, W. J.; Iversen, M. H.; Salter, I. Properties of Sediment Trap Catchment Areas in Fram Strait: Results From Lagrangian Modeling and Remote Sensing. *Front. Mar. Sci.* **2018**, *5*, 407.
(38) Soltwedel, T.; Bauerfeind, E.; Bergmann, M.; Bracher, A.; Budaeva, N.; Busch, K.; Cherkasheva, A.; Fahl, K.; Grzelak, K.; Hasemann, C.; Jacob, M.; Kraft, A.; Lalande, C.; Metfies, K.; Nöthig, E.-M.; Meyer, K.; Quéric, N.-V.; Schewe, I.; Włodarska-Kowalczuk, M.; Klages, M. Natural variability or anthropogenically-induced variation? Insights from 15 years of multidisciplinary observations at the Arctic marine LTER site HAUSGARTEN. *Ecol. Indic.* **2016**, *65*, 89−102.
(39) Engel, A.; Bracher, A.; Dinter, T.; Endres, S.; Grosse, J.; Metfies, K.; Peeken, I.; Piontek, J.; Salter, I.; Nothig, E. M. Inter-Annual Variability of Organic Carbon Concentration in the Eastern Fram Strait During Summer (2009−2017). *Front. Mar. Sci.* **2019**, *6*, 187.
(40) Löder, M. G. J.; Imhof, H. K.; Ladehoff, M.; Löschel, L. A.; Lorenz, C.; Mintenig, S.; Piehl, S.; Primpke, S.; Schrank, I.; Laforsch, C.; Gerdts, G. Enzymatic Purification of Microplastics in Environmental Samples. *Environ. Sci. Technol.* **2017**, *51* (24), 14283−14292.
(41) Löder, M. G. J.; Kuczera, M.; Mintenig, S.; Lorenz, C.; Gerdts, G. Focal plane array detector-based micro-Fourier-transform infrared imaging for the analysis of microplastics in environmental samples. *Environmental Chemistry* **2015**, *12* (5), 563−581.
(42) Redner, S.; Datta, S. Clogging time of a filter. *Phys. Rev. Lett.* **2000**, *84*, 6018−21.
(43) Primpke, S.; Dias, P. A.; Gerdts, G. Automated identification and quantification of microfibres and microplastics. *Anal. Methods* **2019**, *11* (16), 2138−2147.
(44) Mani, T.; Primpke, S.; Lorenz, C.; Gerdts, G.; Burkhardt-Holm, P. Microplastic Pollution in Benthic Midstream Sediments of the Rhine River. *Environ. Sci. Technol.* **2019**, *53* (10), 6053−6062.
(45) Primpke, S.; Wirth, M.; Lorenz, C.; Gerdts, G. Reference database design for the automated analysis of microplastic samples based on Fourier transform infrared (FTIR) spectroscopy. *Anal. Bioanal. Chem.* **2018**, *410* (21), 5131−5141.
(46) Wekerle, C.; Wang, Q.; von Appen, W.-J.; Danilov, S.; Schourup-Kristensen, V.; Jung, T. Eddy-Resolving Simulation of the Atlantic Water Circulation in the Fram Strait With Focus on the Seasonal Cycle. *Journal of Geophysical Research: Oceans* **2017**, *122* (11), 8385−8405.
(47) Kaiser, D.; Estelmann, A.; Kowalski, N.; Glockzin, M.; Waniek, J. J. Sinking velocity of sub-millimeter microplastic. *Mar. Pollut. Bull.* **2019**, *139*, 214−220.
(48) Tippenhauer, S.; Torres-Valdés, S.; Fong, A. A.; Krauß, F.; Huchler, M.; Wisotzki, A., Physical oceanography during POLARSTERN cruise PS99.2 (ARK-XXX/1.2). In *PANGAEA*; 2017.
(49) Krumpen, T. Sea Ice and Amtospheric Conditions at HAUSGARTEN between 2000−2016 (daily resolution), link to model results. In *PANGAEA*; 2017.
(50) Bodungen, B. V.; Wunsch, M.; Fürderer, H. Sampling and Analysis of Suspended and Sinking Particles in the Northern North Atlantic. *Marine Particles: Analysis and Characterization* **2013**, 47−56.
(51) Anderson, M. J.; Walsh, D. C. I. PERMANOVA, ANOSIM, and the Mantel test in the face of heterogeneous dispersions: What null hypothesis are you testing? *Ecol. Monogr.* **2013**, *83* (4), 557−574.
(52) Woodall, L. C.; Sanchez-Vidal, A.; Canals, M.; Paterson, G. L. J.; Coppock, R.; Sleight, V.; Calafat, A.; Rogers, A. D.; Narayanaswamy, B. E.; Thompson, R. C. The deep sea is a major sink for microplastic debris. *R. Soc. Open Sci.* **2014**, *1* (4), 140317.
(53) Tekman, M. B.; Bergmann, M.; Gutow, L. *LITTERBASE*. https://litterbase.awi.de/.
(54) Mu, J. L.; Qu, L.; Jin, F.; Zhang, S.; Fang, C.; Ma, X.; Zhang, W.; Huo, C.; Cong, Y.; Wang, J. Abundance and distribution of microplastics in the surface sediments from the northern Bering and Chukchi Seas. *Environ. Pollut.* **2019**, *245*, 122.
(55) Kanhai, L. D. K.; Johansson, C.; Frias, J. P. G. L.; Gardfeldt, K.; Thompson, R. C.; O'Connor, I. Deep sea sediments of the Arctic Central Basin: A potential sink for microplastics. *Deep Sea Res., Part I* **2019**, *145*, 137−142.
(56) Cincinelli, A.; Scopetani, C.; Chelazzi, D.; Lombardini, E.; Martellini, T.; Katsoyiannis, A.; Fossi, M. C.; Corsolini, S. Microplastic in the surface waters of the Ross Sea (Antarctica): Occurrence, distribution and characterization by FTIR. *Chemosphere* **2017**, *175*, 391−400.
(57) Desforges, J.-P. W.; Galbraith, M.; Dangerfield, N.; Ross, P. S. Widespread distribution of microplastics in subsurface seawater in the NE Pacific Ocean. *Mar. Pollut. Bull.* **2014**, *79* (1), 94−99.
(58) Enders, K.; Lenz, R.; Stedmon, C. A.; Nielsen, T. G. Abundance, size and polymer composition of marine microplastics ≥10mum in the Atlantic Ocean and their modelled vertical distribution. *Mar. Pollut. Bull.* **2015**, *100* (1), 70−81.
(59) Morgana, S.; Ghigliotti, L.; Estévez-Calvar, N.; Stifanese, R.; Wieckzorek, A.; Doyle, T.; Christiansen, J. S.; Faimali, M.; Garaventa, F. Microplastics in the Arctic: A case study with sub-surface water and fish samples off Northeast Greenland. *Environ. Pollut.* **2018**, *242*, 1078−1086.
(60) Barrows, A. P. W.; Cathey, S. E.; Petersen, C. W. Marine environment microfiber contamination: Global patterns and the diversity of microparticle origins. *Environ. Pollut.* **2018**, *237*, 275−284.

https://dx.doi.org/10.1021/acs.est.9b06981
Environ. Sci. Technol. 2020, 54, 4079−4090

(61) Lusher, A.; Tirelli, V.; O'Connor, I.; Officer, R. Microplastics in Arctic polar waters: The first reported values of particles in surface and sub-surface samples. *Sci. Rep.* **2015**, *5*, 14974.
(62) Everaert, G.; Van Cauwenberghe, L.; De Rijcke, M.; Koelmans, A. A.; Mees, J.; Vandegehuchte, M.; Janssen, C. R. Risk assessment of microplastics in the ocean: Modelling approach and first conclusions. *Environ. Pollut.* **2018**, *242*, 1930−1938.
(63) Fazey, F. M. C.; Ryan, P. G. Biofouling on buoyant marine plastics: An experimental study into the effect of size on surface longevity. *Environ. Pollut.* **2016**, *210*, 354−360.
(64) Cathalot, C.; Rabouille, C.; Sauter, E.; Schewe, I.; Soltwedel, T. Benthic Oxygen Uptake in the Arctic Ocean Margins - A Case Study at the Deep-Sea Observatory HAUSGARTEN (Fram Strait). *PLoS One* **2015**, *10* (10), No. e0138339.
(65) Hattermann, T.; Isachsen, P. E.; von Appen, W.-J.; Albretsen, J.; Sundfjord, A. Eddy-driven recirculation of Atlantic Water in Fram Strait. *Geophys. Res. Lett.* **2016**, *43* (7), 3406−3414.
(66) Bakun, A. Climate change and ocean deoxygenation within intensified surface-driven upwelling circulations. *Philos. Trans. R. Soc., A* **2017**, *375* (2102), 20160327.
(67) Codispoti, L. A.; Friederich, G. E.; Sakamoto, C. M.; Gordon, L. I. Nutrient cycling and primary production in the marine systems of the Arctic and Antarctic. *Journal of Marine Systems* **1991**, *2* (3), 359−384.
(68) Wollenburg, J. E.; Katlein, C.; Nehrke, G.; Nöthig, E. M.; Matthiessen, J.; Wolf- Gladrow, D. A.; Nikolopoulos, A.; Gázquez-Sanchez, F.; Rossmann, L.; Assmy, P.; Babin, M.; Bruyant, F.; Beaulieu, M.; Dybwad, C.; Peeken, I. Ballasting by cryogenic gypsum enhances carbon export in a *Phaeocystis* under-ice bloom. *Sci. Rep.* **2018**, *8* (1), 7703.
(69) Cheung, P. K.; Fok, L.; Hung, P. L.; Cheung, L. T. O. Spatio-temporal comparison of neustonic microplastic density in Hong Kong waters under the influence of the Pearl River Estuary. *Sci. Total Environ.* **2018**, *628−629*, 731−739.
(70) Cole, M.; Lindeque, P.; Fileman, E.; Halsband, C.; Goodhead, R.; Moger, J.; Galloway, T. S. Microplastic Ingestion by Zooplankton. *Environ. Sci. Technol.* **2013**, *47* (12), 6646−6655.
(71) Trudnowska, E.; Sagan, S.; Błachowiak-Samołyk, K. Spatial variability and size structure of particles and plankton in the Fram Strait. *Prog. Oceanogr.* **2018**, *168*, 1−12.
(72) Katija, K.; Choy, C. A.; Sherlock, R. E.; Sherman, A. D.; Robison, B. H. From the surface to the seafloor: How giant larvaceans transport microplastics into the deep sea. *Sci. Adv.* **2017**, *3* (8), No. e1700715.
(73) Sun, Y.; Xu, W.; Gu, Q.; Chen, Y.; Zhou, Q.; Zhang, L.; Gu, L.; Huang, Y.; Lyu, K.; Yang, Z. Small-Sized Microplastics Negatively Affect Rotifers: Changes in the Key Life-History Traits and Rotifer−*Phaeocystis* Population Dynamics. *Environ. Sci. Technol.* **2019**, *53* (15), 9241−9251.
(74) ACC. *Elements of the Business of Chemistry*; The American Chemistry Council, 2018.
(75) Oxvig, U. H.; Ulrik, J. *Fishing Gears*; Fiskericirklen, 2007.
(76) Cózar, A.; Martí, E.; Duarte, C. M.; García-de-Lomas, J.; van Sebille, E.; Ballatore, T. J.; Eguíluz, V. M.; González-Gordillo, J. I.; Pedrotti, M. L.; Echevarría, F.; Troublè, R.; Irigoien, X. The Arctic Ocean as a dead end for floating plastics in the North Atlantic branch of the Thermohaline Circulation. *Science Advances* **2017**, *3* (4), No. e1600582.
(77) van Sebille, E.; England, M. H.; Froyland, G. Origin, dynamics and evolution of ocean garbage patches from observed surface drifters. *Environ. Res. Lett.* **2012**, *7* (4), No. 044040.
(78) Schmidt, C.; Krauth, T.; Wagner, S. Export of Plastic Debris by Rivers into the Sea. *Environ. Sci. Technol.* **2017**, *51* (21), 12246−12253.
(79) Cai, P.; Rutgers van der Loeff, M.; Stimac, I.; Nöthig, E. M.; Lepore, K.; Moran, S. B. Low export flux of particulate organic carbon in the central Arctic Ocean as revealed by ^{234}Th:^{238}U disequilibrium. *J. Geophys. Res.* **2010**, *115* (C10), C10037.
(80) Arrigo, K. R.; van Dijken, G. L. Continued increases in Arctic Ocean primary production. *Prog. Oceanogr.* **2015**, *136*, 60−70.
(81) Wassmann, P.; Kosobokova, K. N.; Slagstad, D.; Drinkwater, K. F.; Hopcroft, R. R.; Moore, S. E.; Ellingsen, I.; Nelson, R. J.; Carmack, E.; Popova, E.; Berge, J. The contiguous domains of Arctic Ocean advection: Trails of life and death. *Prog. Oceanogr.* **2015**, *139*, 42−65.
(82) Brandon, J. A.; Jones, W.; Ohman, M. D. Multidecadal increase in plastic particles in coastal ocean sediments. *Science Advances* **2019**, *5* (9), eaax0587.

https://dx.doi.org/10.1021/acs.est.9b06981
Environ. Sci. Technol. 2020, 54, 4079−4090